XV. NEUROLOGY*

L. Stark
F. H. Baker
L. G. Bishop
A. W. England
C. A. Finnila
H. T. Hermann
J. C. Houk
M. King
W. Kipiniak
H. Levy
G. P. Nelson
M. SiK Oh
Y. Okabe
R. C. Payne
N. Perrin
Julia H. Redhead
Helen E. Rhodes
P. R. Samson
G. Sever
I. Sobel
S. F. Stanton
J. N. Thurman
L. A. M. Verbeek
P. A. Willis
L. R. Young

A. SERVOANALYSIS OF THE PUPIL OF THE OWL

1. Introduction

The pupil of the eye is of interest as an example of a neurological servomechanism. The human pupil has already been intensively studied, and in this report we have extended

Fig. XV-1. Max, the Owl (Otus asio).

*This research is supported in part by the U.S. Public Health Service (B-3055, B-3090); the Office of Naval Research (Nonr-609(39)); the Air Force (AF33(616)-7282); and the Army Chemical Corps (DA-18-108-405-Cml-942).

these researches to the pupil of another species.

The owl is an exceptionally good subject because of its large eye and rapid dynamical pupil response. The grave demeanor of the owl is due in part, perhaps, to the lack of eyeball position movements so that the field of vision is changed by rather slow rotations of the head. In fact, we find that if the owl is carefully and comfortably restrained, he does not even move his head but gazes fixedly at our experimental apparatus with only occasional blinks of his inner eyelid. We attempted to work with the Great Horned Owl and the Snowy Owl but found that these large birds of prey are not especially good companions in the dark experimental room. We therefore settled on the screech owl (species: Otus asio) which is only 7 inches tall and much easier to handle. (See Fig. XV-1.) Even the diminutive Screech Owl has a pupillary aperture larger than that of man.

We applied transient and steady-state analysis with an initial departure in terms of small-signal linearization and then proceeded to look at important and interesting nonlinearities. Of especial interest was the comparison of the human and owl pupillary systems in terms of both frequency response and nonlinearities.

2. Experimental Method

The experimental method used exploits the advantages of the pupil system. The retina of the eye is easily and painlessly stimulated by an electronically controlled light

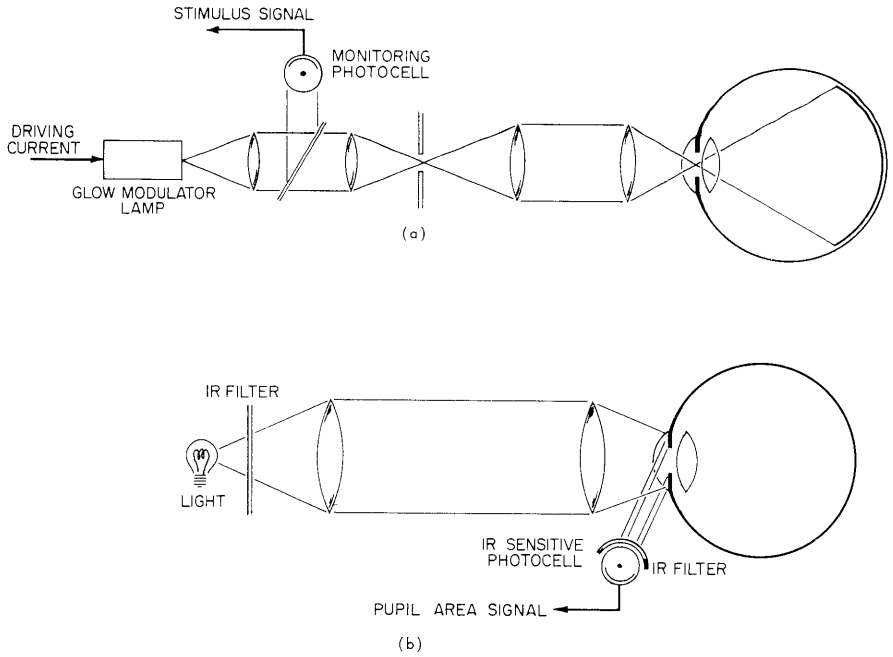

Fig. XV-2. Pupilometer showing two main portions: (a) stimulating light; (b) infrared light with area-measuring system used.

source as shown in Fig. XV-2a. Open-loop operating conditions were obtained by focusing the light at the plane of the pupil to a disc smaller than the smallest area of the pupil. Pupil area was measured with invisible infrared light[1] and an infrared photocell as shown in Fig. XV-2b. The recording system was calibrated by means of several flash photographs; thus photocell current could be directly interpreted as pupil area. Complete details of pupilometer apparatus have been published.[2]

The voltages representing input (light) and output (area) were either recorded on rectilinear paper chart recorders, on magnetic tape recorders, or run directly into the RW-300 digital computer for analysis.

3. Experimental Findings

Several examples of transient responses of the owl's pupil are shown in Fig. XV-3. Among the points to be noted are the short latent period which in the owl is 0.5-0.10 sec

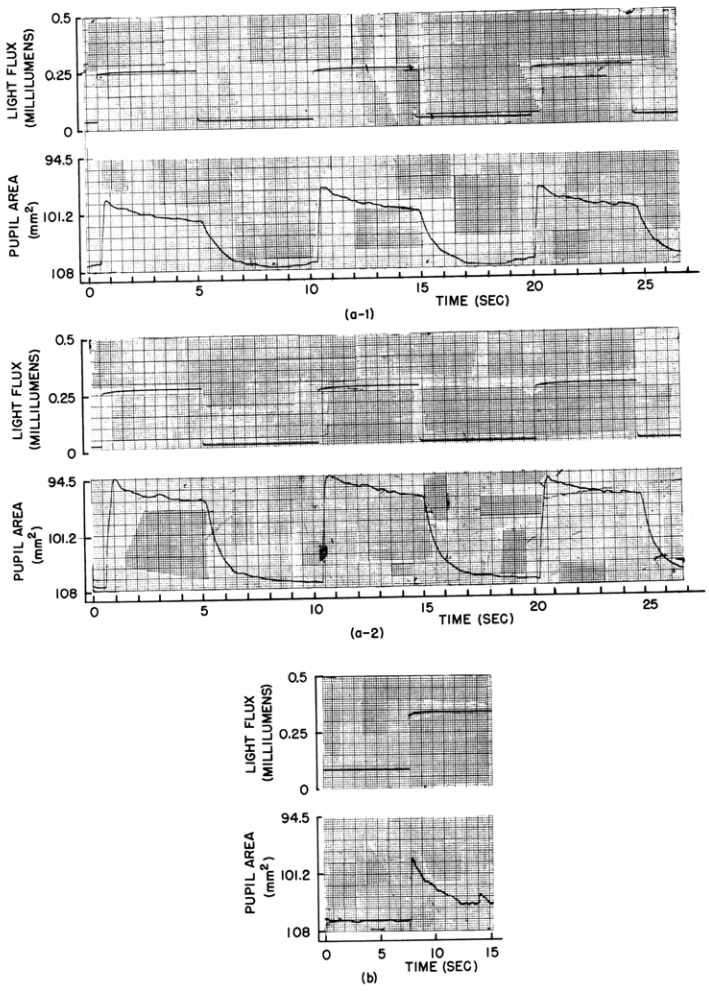

Fig. XV-3. Time functions showing responses to step changes in light (open-loop).

for constriction, and 0.15-0.2 sec for dilatation. In the human these values are 0.20 sec for constriction, and more than 0.2 sec for dilatation. There is also a high velocity of constriction as compared with the human. This velocity of constriction is greater than the velocity of dilatation, and this asymmetry is also seen in the human. It can be seen, by changing input amplitudes (Fig. XV-3a-1 and XV-3a-2) so as to obtain different response amplitudes, that the time constants discussed above are dependent upon amplitude. Occasionally marked overshooting and ringing can be seen (Fig. XV-3b).

Adaptive processes that probably represent retinal light adaption can be seen after constriction, and even the time constants of these adaptive processes are dependent upon amplitude.

Noise is much less apparent in these time-function recordings of the owl than in human pupillary records. However, it also seems to occur in the constricted phase with larger amplitude than in the dilated phase. The variability of the system from response to response is apparent and is characteristic of the nonstationariness of these biological systems. By performing experiments wherein the amplitude of the light step, as well as the mean level of light, is changed in order of magnitude by means of neutral density filters, it becomes apparent that the effective stimulus is a percentage change of light amplitude rather than an absolute value.

In Fig. XV-4 some examples of steady-state responses are shown. Among the points to be noted in this figure is that most of the power is in the fundamental frequency component. The response represents small fluctuation in pupil area of approximately 10 per cent, or less, and it therefore seems reasonable to apply small-signal linearization techniques. By observing the input frequency and the amplitude and phase lag of the iris response, it can be seen that the system has the general characteristics of a low bandpass filter. Asymmetries, variability, and noise can also be seen in these records, and our report will present experiments designed to elucidate some of these nonlinearities.

4. Frequency Response Analysis and Transfer Function

A series of experiments, as shown in Fig. XV-4, can be used to obtain gain and phase lag as a function of frequency. These data were obtained and presented in the form of the Bode plot of Fig. XV-5.

Gain is defined as the ratio of the change of flux produced by change in the pupillary aperture (F_p) to the change of flux produced by change in external light intensity (F_s). This can be further broken down to the relationships between changes in area and light intensity and mean area and mean intensity as shown in Eq. 1.

$$G = \frac{\Delta F_p}{\Delta F_s} = \frac{\Delta A \cdot \bar{I}}{\Delta \bar{I} \cdot \bar{A}} = \frac{\Delta \bar{A}/\bar{A}}{\Delta \bar{I}/\bar{I}} \tag{1}$$

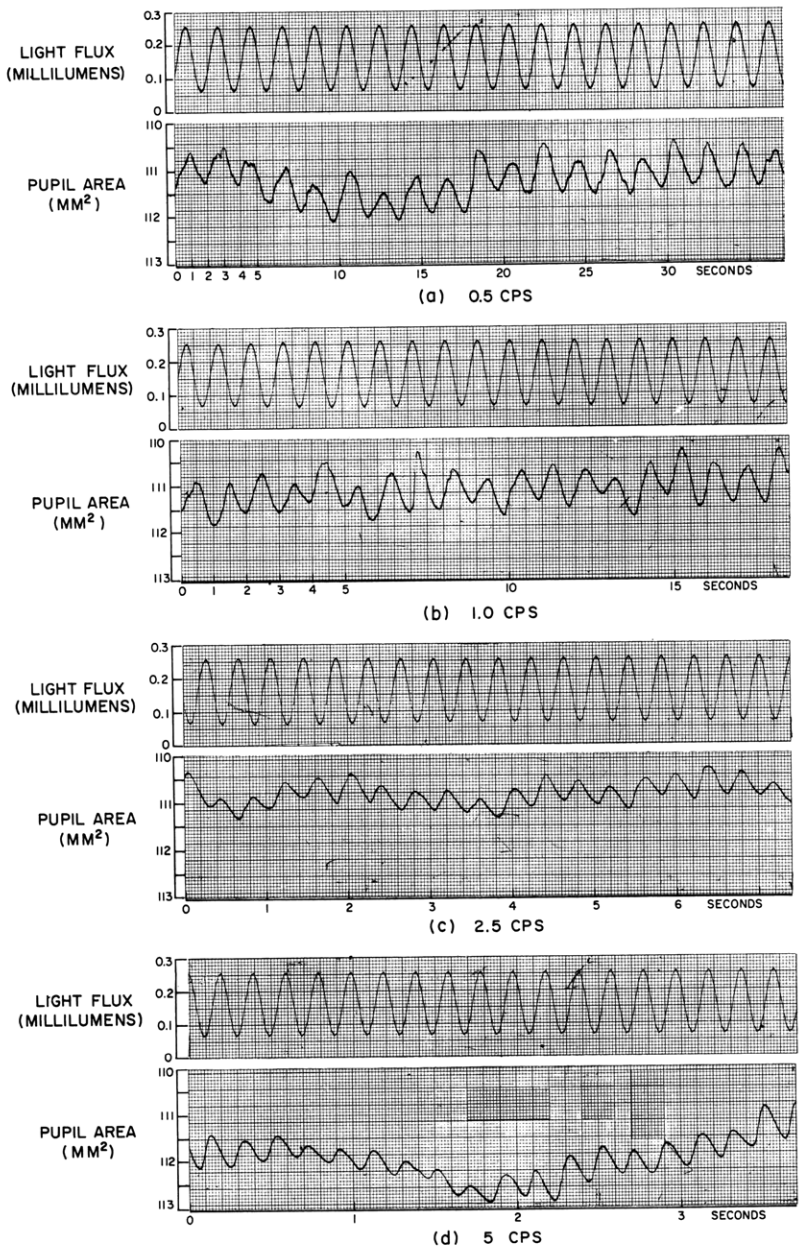

Fig. XV-4. Time functions showing response to sinusoidal changes (open-loop).

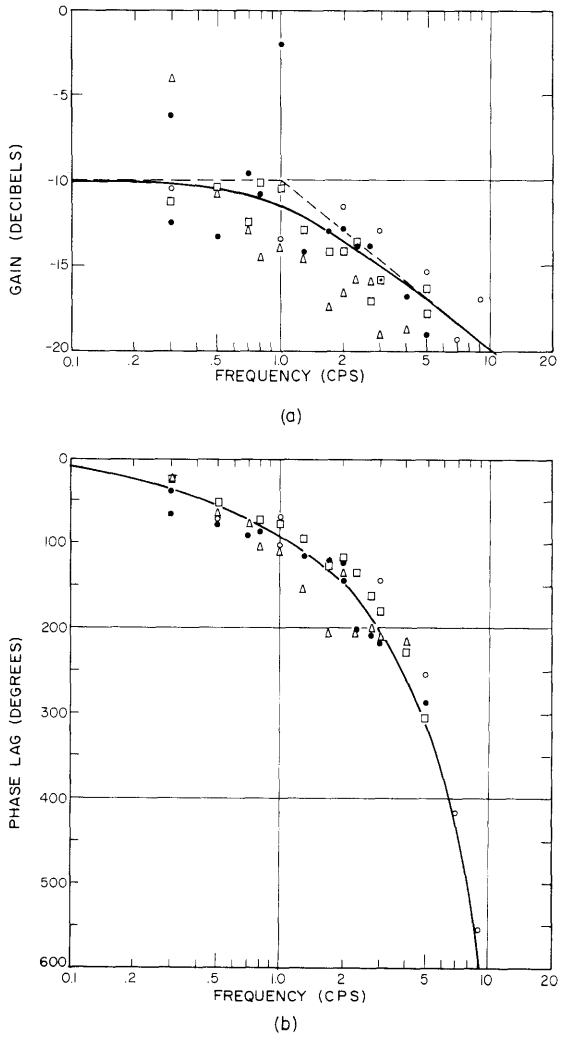

Fig. XV-5. Bode plot. Asymptotes from transfer function.
Key: ▭, Run No. 1.
Δ, Run No. 2.
•, Run No. 3.
O, Run No. 4.

Upon examining Fig. XV-5 several interesting features can be observed. First, low-frequency and mid-frequency gain is quite low. This predicts that the open- and closed-loop gain will not be very different, an experimental fact observed by us. There is a break frequency at 1 cps, and then an attenuation that asymptotically approaches a slope of -1 or 10 decilogs per decade (6 db per octave).

The phase characteristics shown in Fig. XV-5 indicate that in addition to the minimum phase lag element, which accounts for the attenuation slope, there is also a non-minimum phase lag element. The minimum phase lag element is due most likely to the physiological mechanism involved in moving the thin sheet of iris muscle in the anterior

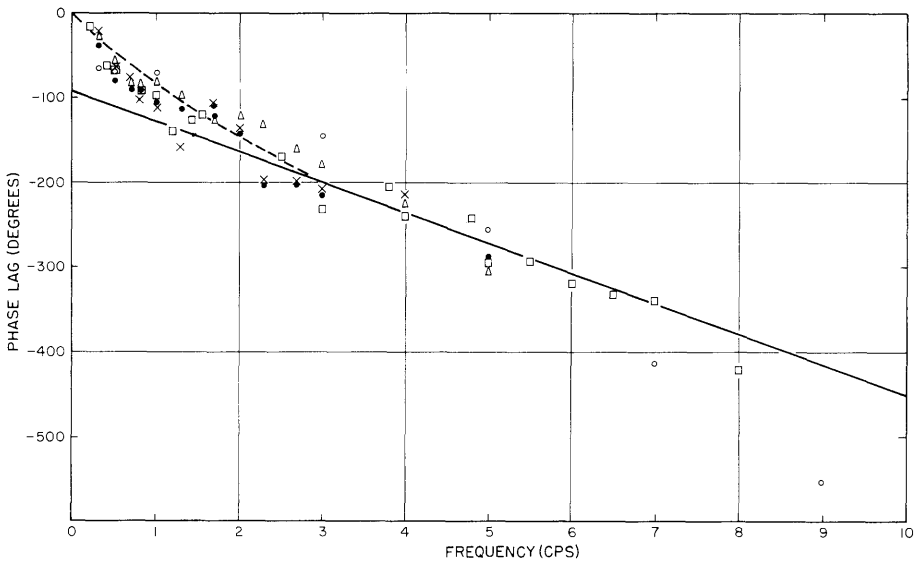

Fig. XV-6. Phase lag as a function of linear frequency.
Key: × , Run No. 1.
□ , Run No. 2.
△ , Run No. 3.
● , Run No. 4.
○ , Run No. 5.

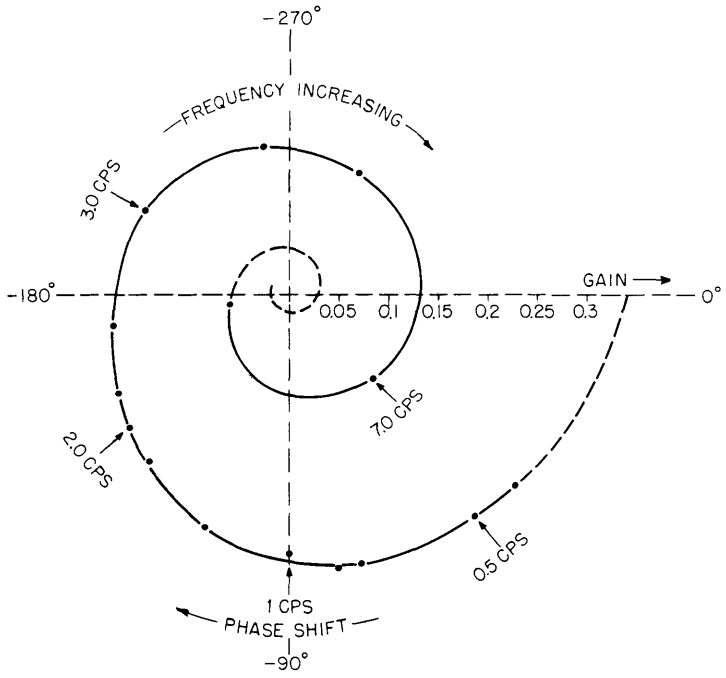

Fig. XV-7. Nyquist plot.

chamber of the eye lying between the lens and the cornea. The scatter of the points indicates nonstationariness of the pupillary system and also moderate change in operating conditions from experiment to experiment.

In Fig. XV-6 is plotted linear phase lag vs linear frequency. A nonminimum phase lag element corresponding to the latent period seen in the step responses should produce a characteristic functional relationship, as shown by the dashed line. It can be seen that after the minimum phase lag element has already contributed its phase lag of 90° the experimental data approximate this slope.

From these graphical frequency-response displays we can construct a transfer function representing a linear lumped parameter approximation to the pupillary system over the frequency range studied.

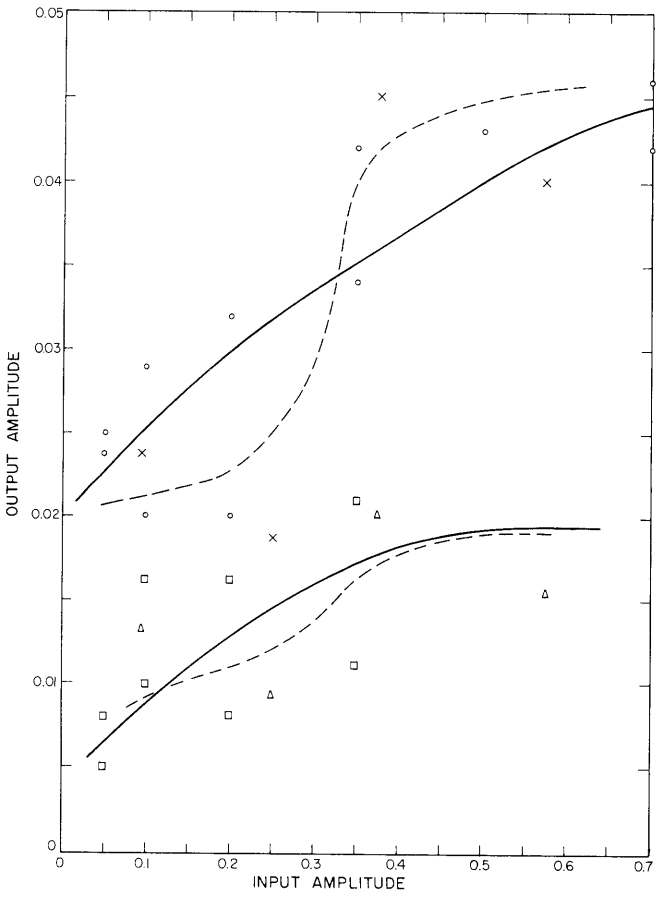

Fig. XV-8. Output amplitude as a function of input amplitude. Owl and human at two frequencies.
Key: --x--Owl, 0.6 cps.
--Δ--Owl, 2.0 cps.
—o—Human, 0.6 cps.
—□—Human, 2.0 cps.

$$G = \frac{0.1\, e^{-0.1s}}{(1+0.15s)} \qquad (2)$$

This consists of a low-frequency gain, a transport delay, and a simple lag element. The asymptotes drawn for Figs. XV-5 and XV-6 represent this transfer function, and adequacy of the fit of the delay can be judged by referring to these figures.

The Nyquist curve shown in Fig. XV-7 is another display of the pupil system features. On this vector plot of gain and phase lag the stability characteristics of the system can be seen.

5. Nonlinear Characteristics

Because of the importance of the nonlinearities and asymmetries of the pupillary system of the owl, we felt that it was important to include a preliminary description in this first report.

a. Frequency-Independent Features

It has been suggested that certain nonmemory nonlinearities are important features of the human pupillary system. By reference to Fig. XV-8 it can be seen that there is an important saturation characteristic that holds over the entire input range. The saturation is approximately logarithmic or, even more steeply, a function of input amplitude. In this way the human pupil reacts with a gain of up to 0.6 to small inputs in the mid-frequency range. It pays for this higher gain by responding very little to a second and even larger stimulus in the same direction as the initial one.

The owl, on the other hand, shows a "dead space" phenomenon whereby the response to large inputs is much more than proportionally decreased for small inputs over an important portion of the range. This phenomenon is shown in Fig. XV-8 and can also be seen in the time-function data shown in Fig. XV-9.

b. Static Characteristics

At this point it may be well to mention some static features of the two pupillary systems, the owl and the human. The owl has an extreme range of 6-115 mm^2 and the usual operating range under our experimental conditions of fairly bright light was 95-115 mm^2. The extreme range of the human pupil is approximately 2-40 mm^2, and under similar experimental conditions the usual operating range is 16-30 mm^2. This is a rather striking difference both with regard to extreme size and to usual size under our experimental conditions. We cannot explain why the owl, a nocturnal species, has a dilated pupil under conditions of our experimental stimulation with moderately bright lights.

The fact of this dilatation leads to a prediction that an effect of gain change would be to change the mean size of the pupil. For example, increasing gain must increase

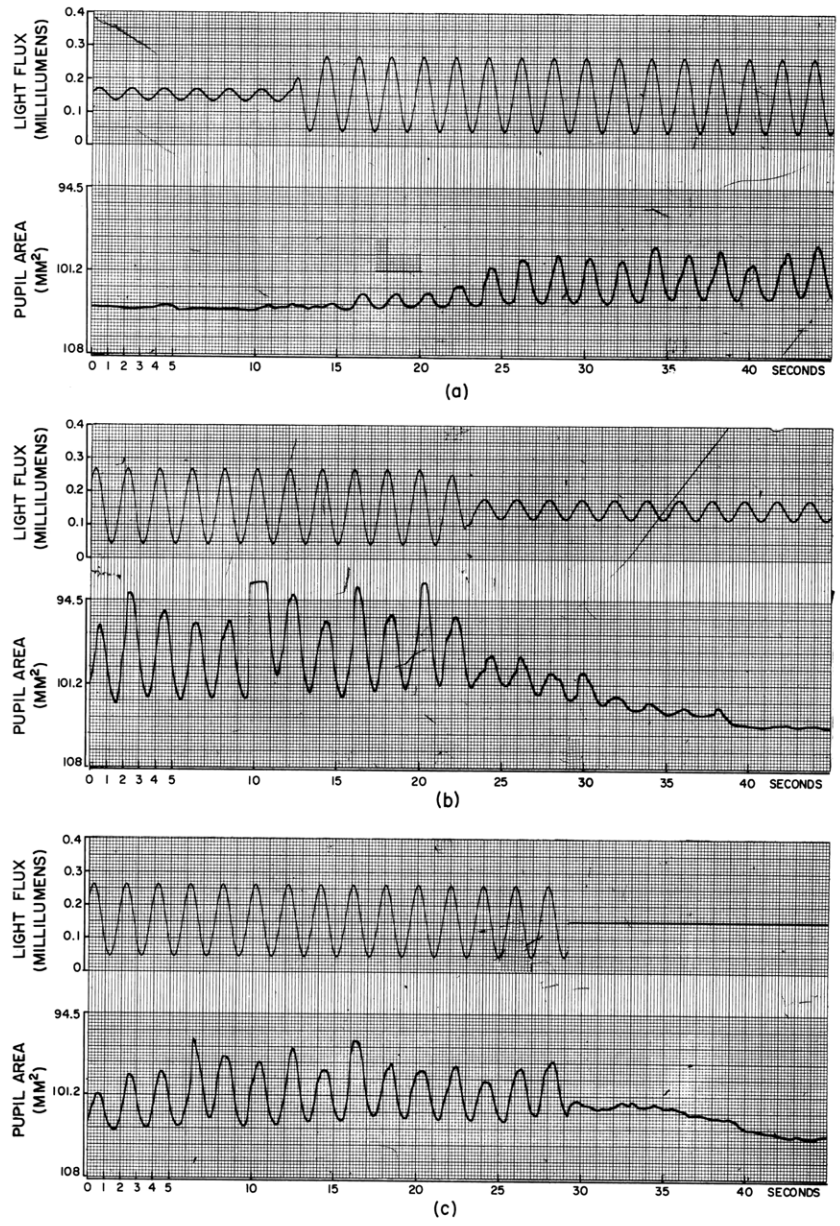

Fig. XV-9. Time functions showing response to sinusoidal changes, and especially to step changes of amplitude of the sinusoidal inputs. (a) Increasing amplitude. (b) Decreasing amplitude. (c) Decreasing amplitude to zero.

output amplitude. Output amplitude can only be changed when the pupil is fully dilated at one end of the driven oscillation by further constricting the pupil at the other end of the driven oscillation. This, in turn, will have the effect of decreasing the mean level of pupil area.

Figure XV-9 shows an experiment in which confirmation of this prediction is observed. Here the increased gain results in constricting the pupil.

c. Time-dependent Amplitude Changes

Another series of experiments related to the one above shows the marked complexity of the actual control system of the owl pupil. It will be noted in Fig. XV-9 that the change in response amplitude lags behind the change in stimulus amplitude with a time constant of approximately 3 seconds. Figure XV-9b shows that this also occurs in the reverse direction.

One possible explanation of this time-dependent amplitude change might be delays caused by a fairly high Q filter. It might be that the owl adjusts the bandwidth of its pupil-control system to fit the bandwidth of the input signal, and with a stimulus that is a pure sinusoid, this could result in a very high Q filter.

Figure XV-9c clearly disproves this hypothesis. Here the input amplitude is suddenly switched to zero and pupillary response quickly follows suit.

6. Discussion

The pupil of the owl is larger but the gain of 0.1 is not greater than that for the human pupil and similarly provides for stability in spite of large phase lags. The frequency response is approximately 1.5 octaves higher in the owl and transport lags are shorter. The nonlinearities are sometimes in opposite directions. The owl pupil shows relatively larger responses at mid-amplitude, while the human pupil, heavily saturated, responds optimally to very small external light changes. Marked asymmetries, which are due to differing retinal adaptation time constants, are present and similar in both species. Noise is less in the owl.

Both systems show complexity in nonlinear dynamics which is worthy of study in itself and is illustrative of control systems shaped by evolutionary forces to some optimum performance.

7. Conclusion

The methods of linear and nonlinear servoanalysis have proved to be fruitful in design and interpretation of experiments on the pupil of the owl. Expecially rewarding are comparisions of the owl system with the previously studied human pupil.

We wish to thank Professor Bernard Abbott, Department of Zoology, University of California in Los Angeles, for arranging for one of us, Lewis G. Bishop, to work at M.I.T. this summer, and also The Sperry Rand Research Center, Sudbury,

Massachusetts, for providing a predoctoral fellowship for support of this work.

We also want to thank Dr. A. Morgan and Dr. J. Baird of the Audubon Society, Lincoln, Massachusetts, for lending us two screech owls, as well as giving much advice on their handling.

L. G. Bishop, Julia H. Redhead, L. Stark

References

1. Occasionally we used a different set of filters which passed far red visible light. This acted as a small dc stimulating light level; but no significant changes in dynamic characteristics were noted as compared with the true invisible infrared system.

2. L. Stark, Stability, oscillations and noise in the human pupil servomechanism, Proc. IRE 47, 1925 (1959).

B. DYNAMICAL RESPONSE OF THE MOVEMENT COORDINATION SYSTEM OF PATIENTS WITH PARKINSON SYNDROME

1. Introduction

Parkinson syndrome is a common affliction, especially of elderly persons, well known in the neurological literature for the past hundred years. The muscles and nerves of Parkinson patients are generally not at all affected by the disease (until late secondary changes occur). Evidence for this comes from observation of patients who were able to walk normally when sleep walking, as well as from the ability of certain brain operations to modify this syndrome. Approximately thirty-five years ago, it was demonstrated that interruption of the stretch reflex markedly reduced the rigidity which is a prominent sign of this syndrome.[1,2] Recently, as a result of studies of the neurological organization of the control system of movement of normal subjects, a model of much of this system was put forward.[3]

Here it is suggested that the voluntary control for moderate and rapid movements operates in an open-loop fashion, whereas postural tone and end-of-movement damping and clamping operates through a feedback path through the muscle spindles. The diffuse anatomical organization of the gamma input is well suited for this postural feedback system but argues against a follow-up servo-system operation (put forth by Merton[4]).

The following experiments were performed on a series of 20 Parkinson patients and provide further evidence concerning both the nature of the defect of Parkinson syndrome and the organization of the normal control system.

2. Method

The experimental method employs the motor coordination testing apparatus shown in Fig. XV-10 in order to quantify tracking inputs and responses under a variety of handle

impedance conditions. This aspect of our method has been fully described by Stark, Iida, and Willis.[5,6] The apparatus, in general, provides for monitoring and recording of positions, velocities and forces of excitation signals, and response or spontaneous movements. Other types of input besides tracking signals are possible. For example, the subject may be asked to hold the handle but not to resist any movement of the handle caused by the servo motor controlling its position. This is similar to the action of a neurologist in testing a patient's "tone." Instead of subjectively judging the resistive force or "tone" of the patient, we could measure the actual force by means of transducers in the apparatus.

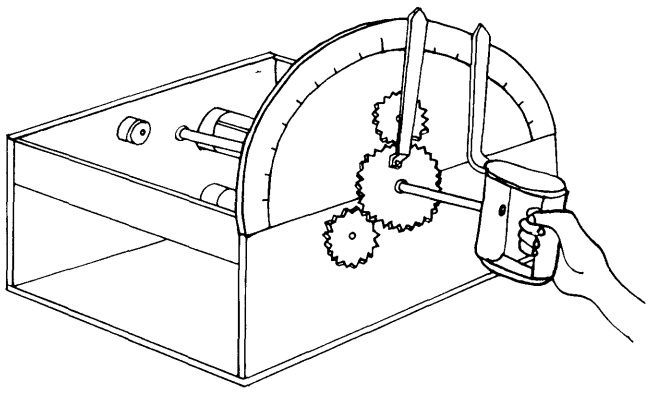

Fig. XV-10. Mechanical portion of the apparatus.

Another form of operation of this apparatus, also described elsewhere,[5,6] is by means of oral instructions to the patient to perform rapid succession movements called "freewheeling." This is similar to a portion of the neurological examination which attempts to elicite signs of dysdiadochokinesis.

3. Experimental Results

a. Frequency Response Data

By performing a series of unpredictable tracking experiments, the frequency response of the human subject can be studied. It is important, as shown by Stark, Iida and Willis,[5,6] to clearly eliminate the predictive ability of the brain if consistent data relating to the "neurological control system" are to be obtained. An example of such frequency-response data is shown in Figs. XV-11 and XV-12. Here, the gain and phase lag are plotted as a function of frequency. The responses of three subjects are shown: a normal person and two patients with mild and moderate degrees of Parkinsonian rigidity. It can be seen that the bandwidth of the patients is severly restricted. This is

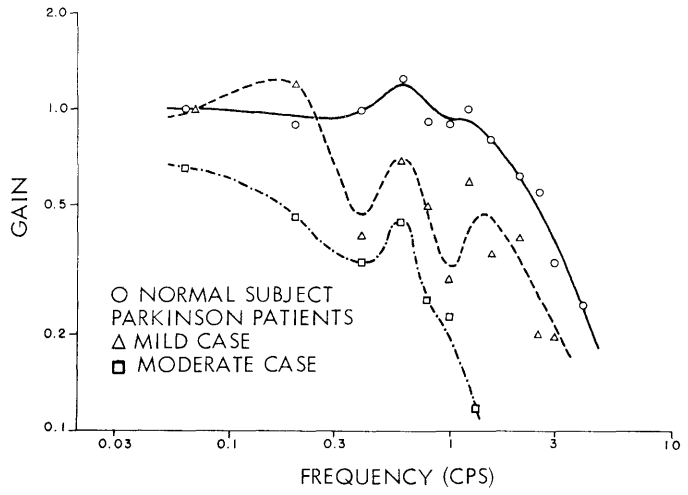

Fig. XV-11. Frequency-response gain data.

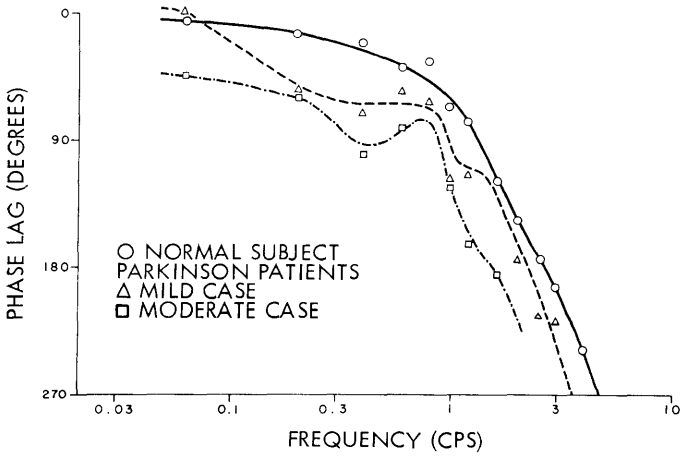

Fig. XV-12. Frequency-response phase data.

consistent with the model of a higher gain postural feedback system operating against voluntary control of the muscles.

The Nyquist diagram shown in Fig. XV-13 is another display of these same data and shows in even more striking form the marked reduction in performance associated with Parkinsonism.

b. Voluntary Strength

Although, as mentioned above, there seems to be no muscular pathology in Parkinson's syndrome, a marked reduction of voluntary strength exists, as shown in

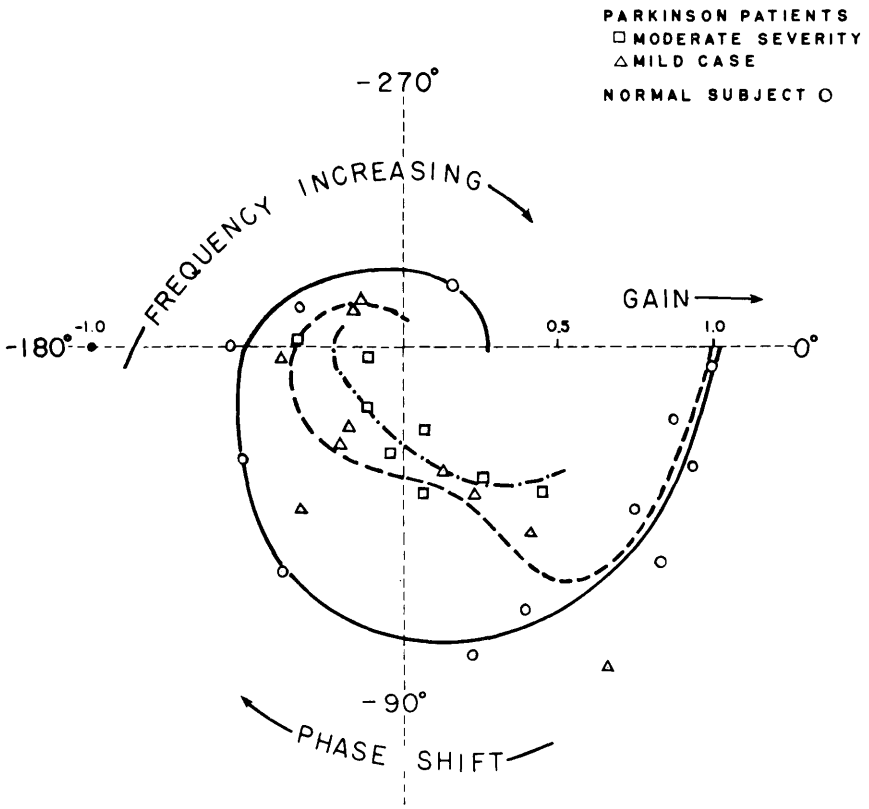

Fig. XV-13. Nyquist diagram (closed loop, unpredictable inputs).

in Table XV-1 and Fig. XV-15. The model predicts this as a consequence of the opposing forces of agonist and antagonistic muscles activated in a contradictory fashion by the not-to-be switched off postural servomechanism.

c. Freewheeling

The decrease in performance also affects the ability of the patient to perform rapid succession movements. In Fig. XV-14 the contrast between two normal subjects and two patients is marked. Later, it will be shown that another aspect of the Parkinson syndrome, tremor, may also influence this behavioral loss.

d. Group Comparisons

A number of Parkinson patients and normal subjects were studied, and from the entire experimental measurement procedure several critical parameters were extracted: the strength in kilograms obtained with voluntary wrist rotation, the freewheeling frequency in cycles per second, and the 180° phase crossover frequency in cycles per second obtained from the frequency-response data described above. These parameters

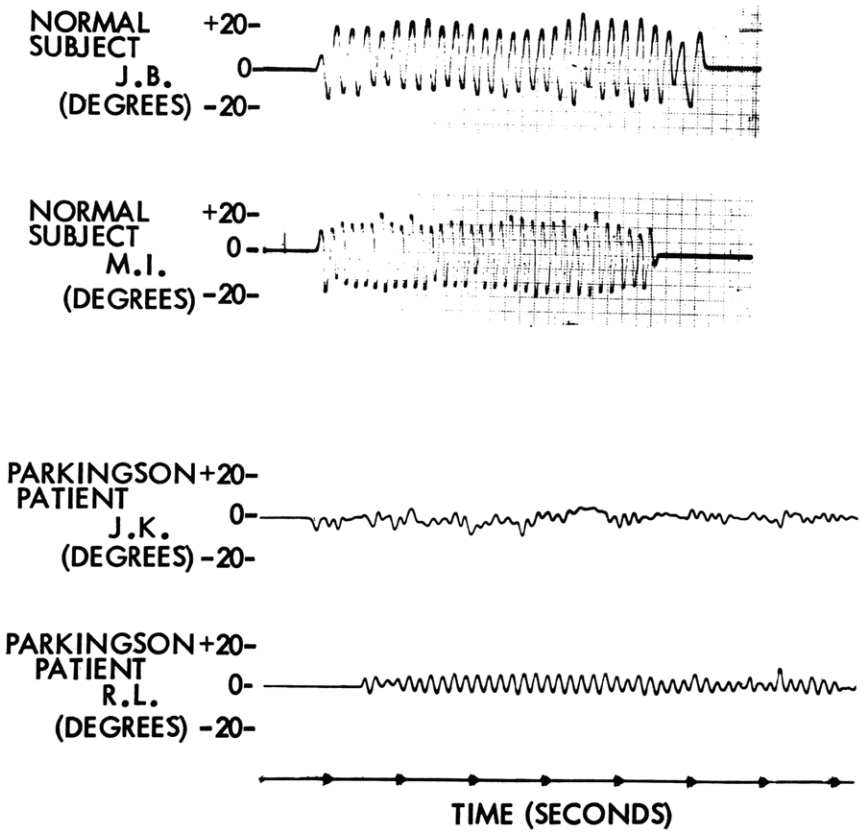

Fig. XV-14. Freewheeling experiment.

are presented in Table XV-1 and also displayed in graphic form in Fig. XV-15. From Fig. XV-15 it can be seen that all three parameters show marked correlation, as well as a striking difference between normals and patients. The 180° phase crossover frequency seems to show fewer false negatives. (In fact, the left hand in patient No. 3 was considered asymptomatic by clinical neurologists.)

e. Tone Experiments

When the "tone" of a subject's muscles was tested, as described in section 2, we found that care had to be exercised to insure that the subject was cooperating as well as possible. Experimental records of simultaneously measured hand displacement and resultant resistive force are shown in Fig. XV-16. We use both sinusoidal and triangular inputs of displacement because of our desire to compare our results with those of previous workers.[7,8] The most apparent result is the larger amount of resistive force obtained from the patient group. This "rigidity" has long been known as an important part of the neurological description of the Parkinson syndrome. Previous theories have ascribed this either to a viscous resistance in the muscles or to an analogous viscous

Table XV-1. Normal and patient group comparisons.

	STRENGTH IN KILOGRAMS		FREE WHEELING FREQUENCY IN CPS		180° PHASE CROSSOVER FREQUENCY IN CPS	
PARKINSON PATIENTS	LEFT	RIGHT	LEFT	RIGHT	LEFT	RIGHT
1. C.M.	1.8	7.3	1.2	2.0	1.7	1.5
2. J.B.	14.1	9.1	0.3	0.3	1.6	1.7
3. S.S.	18.2	18.2	3.0	2.7	3.0	2.3
4. J.K.	10.8	10.0	1.0	2.9	1.6	2.0
5. R.L.	15.4	15.4	2.5	6.0	1.5	1.4
6. A.S.	22.5	22.5	4.0	7.0	2.3	2.3
7. A.C.	2.7	2.7	2.0	1.0	—	—
8. J.P.	8.4	2.7	2.0	4.0	—	—
9. H.B.	10.9	14.5	6.0	6.0	2.1	2.1
10. S.B.	5.6	9.1	2.3	3.3	2.1	1.8
11. J.A.	14.6	18.2	3.0	3.5	2.0	2.0
Average	11.4	11.8	2.5	3.5	2.0	1.9
NORMAL SUBJECTS						
1. M.I.	22.5	22.5	7.0	7.8	2.9	3.2
2. P.W.	22.5	22.5	6.3	7.0	2.8	2.8
3. D.W.	22.0	22.0	6.0	6.4	2.8	2.8
4. T.A.	17.0	17.0	5.7	5.9	2.9	2.9
5. M.M.	20.0	22.0	5.3	6.0	2.6	2.7
6. J.B.	16.0	17.0	5.2	5.5	2.7	2.6
Average	20.0	20.5	5.9	6.4	2.8	2.8

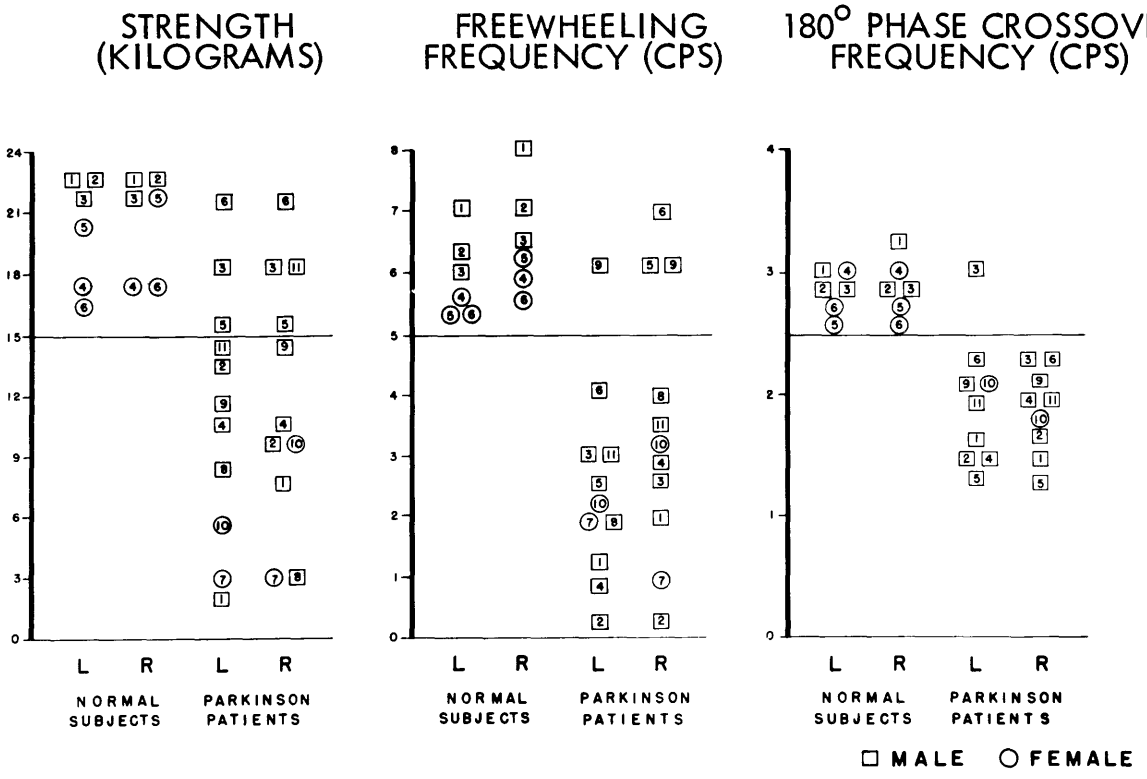

Fig. XV-15. Normal and patient group comparisons.

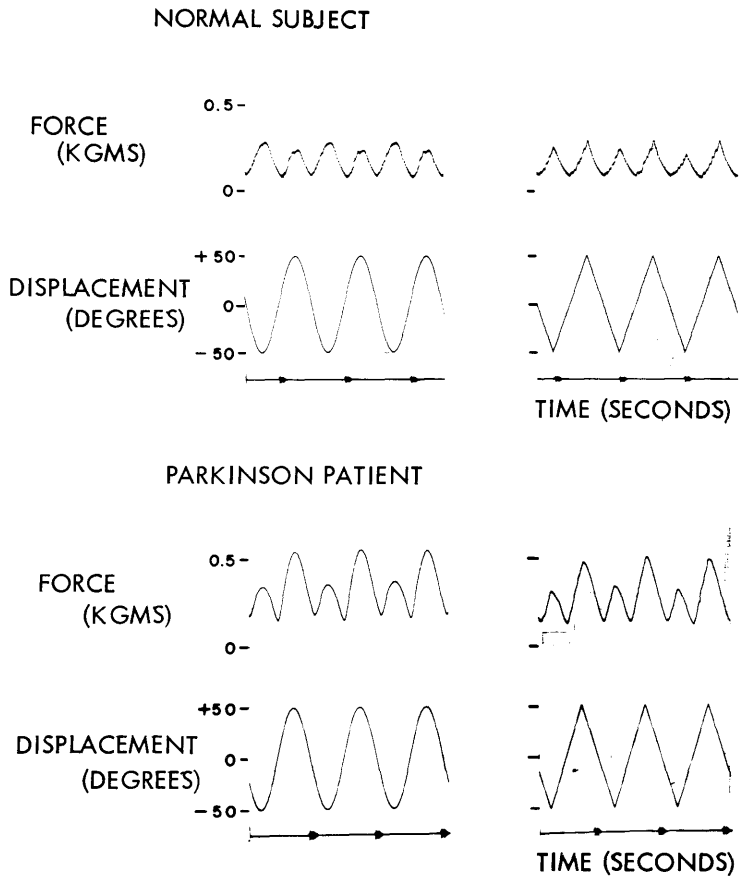

Fig. XV-16. Tone experiment.

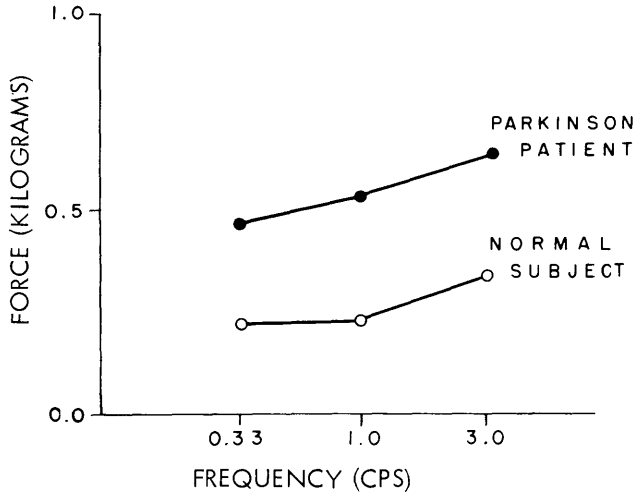

Fig. XV-17. Tone experiment, frequency dependence.

resistivity arising from some neurological reflex reaction. From inspection of Fig. XV-16 it can be seen that the force is in phase with the displacement. Thus, rigidity is entirely an increase in elastic force. This is also true for the smaller resistive forces found in normal subjects.

Further evidence for this comes from the experiment shown in Fig. XV-17 in which it is seen that the rigidity force is not highly frequency-dependent as would be expected if it had a viscous component.

The model for the control of normal movement and posture discussed in this report and its explanation of Parkinson rigidity require this resistive force to be an elastic one. This is so because according to our hypothesis it is due to a postural reaction of the stretch reflex to a displacement error in the length servo, and so results in a force proportional to error and thus to displacement.

The elastic force clearly demonstrated in these tone experiments constitutes evidence in favor of the model.

f. Step Responses and Tremor

Certain time-function records, although they have not yet been used in further

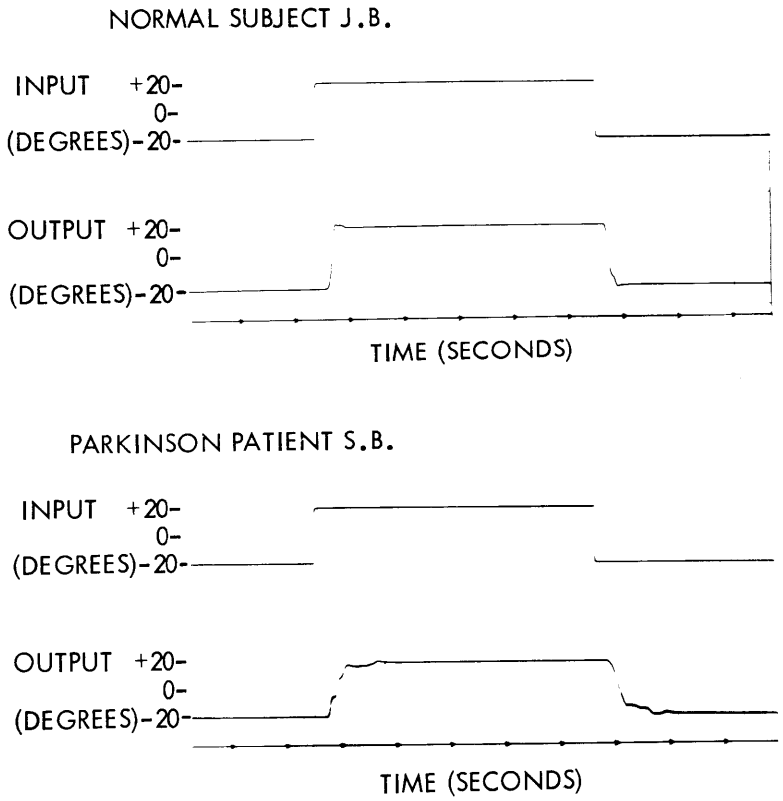

Fig. XV-18. Step experiment.

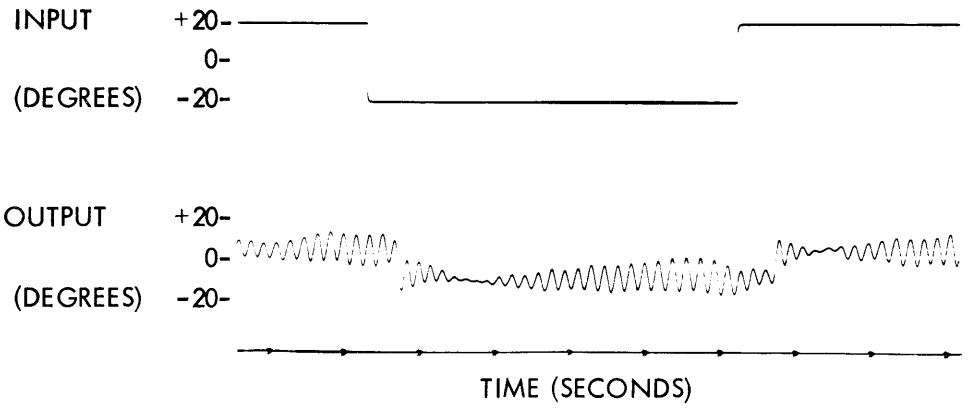

Fig. XV-19. Tremor superimposed on step response.

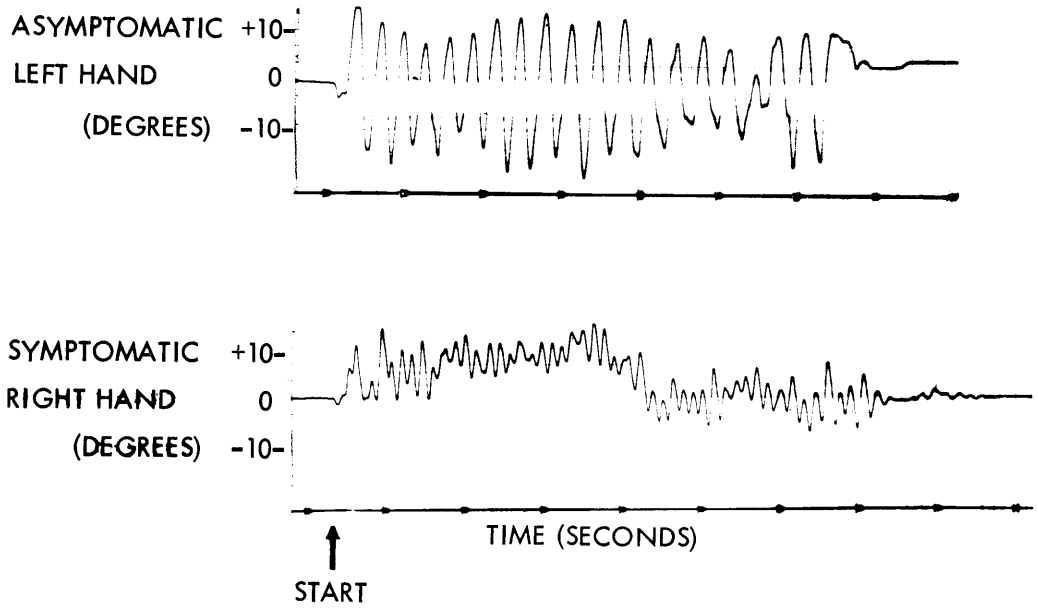

Fig. XV-20. Tremor development during freewheeling.

analytic studies, are of value in terms of a qualitative description of the Parkinson syndrome. Figure XV-18 shows responses of a normal subject and a Parkinson patient to a step input. The slowed irregular response of the patient correlates with the diminished frequency response and lower freewheeling frequency described above.

The normal subject is able to shut off his postural servomechanism when making a voluntary movement. This occurs so rapidly that its site of action is most likely at or near the alpha motor neuron. The Parkinson patient, unable to reduce the gain of his postural servo, must share control of the muscles during volitional movement with contradictory control of the same muscles by the postural servomechanism.

Parkinson syndrome is more complex a disorder than can be possibly explained with our present knowledge.[9] For example, tremor still eludes the neurophysiologist, although the presence of this clear oscillation is tantalizing. In addition to the presence of the rest tremor, the interaction of this tremor with volitional movements is unpredictable and erratic. Figure XV-19 shows an instance of tremor superimposed on a step response. The response of the patient is slowed and inaccurate. Surprisingly, after the movement is completed, the tremor dies down for approximately half a second. On the other hand, as shown in Fig. XV-20, tremor can develop during the performance of a voluntary movement. Here is contrasted freewheeling of the patient's asymptomatic left hand with the development of tremor in the right hand at approximately twice the frequency of the initial abortive freewheeling attempts. When the subject no longer attempts to freewheel the tremor dies down. Professor Robert Schwab, of Massachusetts General Hospital, has shown further difficulties in initiating complex movement which are in addition to the defects ascribable to simple rigidity.

4. Conclusions

The set of experiments described in this report attempts to study the defect in movement coordination present in patients with Parkinson syndrome from the viewpoint of servomechanism theory.[10] It is shown that by taking advantage of known anatomical, physiological, and neurological information, and by orgainzing and interrelating this information from the viewpoint of servoanalysis one can obtain a consistent model that predicts these important and central phenomena:

(i) increased elastic resistance known as rigidity;

(ii) decreased frequency response of voluntary movement demonstrable in tracking experiments;

(iii) deficit in performance of succession movements; and

(iv) decrease in voluntary strength.

L. Stark, M. Iida

References

1. F. M. R. Walsh, Muscular rigidity of paralysis agitans, Brain 47, 159 (1924).

2. L. J. Pollock and L. Davis, Muscle tone in Parkinsonian states, Arch. Neurol. Psychiat. 23, 303-317 (1930).

3. Y. Okabe, R. C. Payne, H. Rhodes, L. Stark, and P. A. Willis, Use of on-line digital computer for measurement of a neurological control system, Quarterly Progress Report No. 61, Research Laboratory of Electronics, M. I. T., April 15, 1961, pp. 219-222.

4. P. A. Merton, Speculations on the servocontrol of movement, The Spinal Cord, A Ciba Foundation Symposium, London, 1953, pp. 247-260.

5. L. Stark, M. Iida, and P. A. Willis, Dynamic characteristics of the motor coordination system in man, Biophys. J. 1, 279-300 (1961).

6. L. Stark, M. Iida, and P. A. Willis, Dynamic characteristics of motor coordination, Quarterly Progress Report No. 60, Research Laboratory of Electronics, M.I.T., January 15, 1961, pp. 231-233.

7. D. D. Webster, Dynamic measurement of rigidity, strength, and tremor in Parkinson patients before and after destruction of mesial globus pallidus, Neurology 10, 157-163 (1960).

8. B. Boshes, H. Wachs, J. Brumlik, M. Mier, and M. Petrovick, Studies of tone, tremor, and speech in normal persons and Parkinsonian patients, Neurology 10, 805-813 (1960).

9. R. S. Schwab, A. C. England, and E. Peterson, Akinesia in Parkinson's disease, Neurology 9, 65-72 (1959).

10. Dr. Mitsuo Iida is now in the Neurology Department, Nagoya University, Japan. We would like to thank Prof. Gilbert Glaser, Head of the Neurology Department, Yale University, where most of this work was carried out. We would also like to thank Dr. Glaser and Dr. Lewis Levy for providing volunteer patients, and to thank the patients themselves for putting up with inconvenience and discomfort in our laboratory. Mr. Paul A. Willis helped greatly throughout these experiments.

C. COMPUTER ANALYSIS OF HANDWRITING

A considerable body of evidence, taken with all normal precaution, attests to the existence of a high correlation between certain features of handwriting and cancer. The aim of this research was to program a digital computer to make the measurements on handwriting needed for detection of cancer.

Previous computer-aided handwriting studies have employed two types of input transducer – one that transmits the instantaneous position of the writing stylus, and another that scans previously recorded writing. The second type was adopted for this research, mainly because of the ease of obtaining data for it. A photomultiplier device was used with the TX-0 computer to scan input data, which were written on transparent plastic.

The scanning program differentiates the photomultiplier output and thus forms a list of the points on the edges of the input writing. Such scanning does not preserve the time ordering of the points, which is essential for further analysis. A synthetic time ordering, sufficient for analysis, is imposed by a program that traces along connected paths of the scanned data.

The most significant features measured in previous work are the change of thickness at points where the vertical direction of the stroke changes, and the curvature of this transition region. A program was written to measure these characteristics, operating on data prepared by the scanning and continuity-tracing programs. This program locates transition regions, measures the thickness on either side, and claculates the

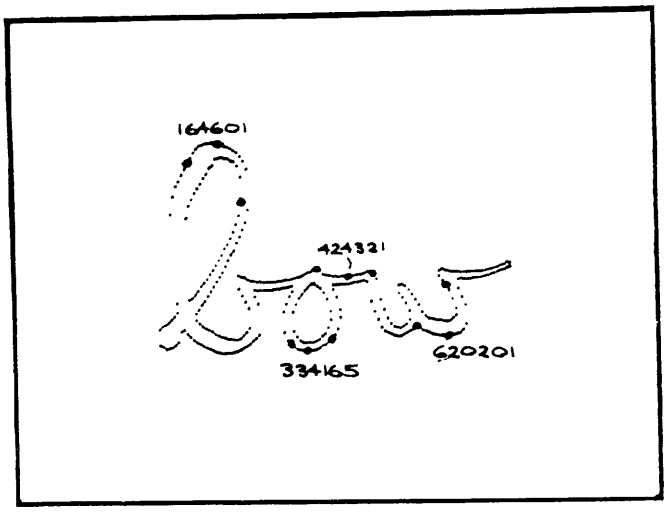

Coordinate	Thickness – s	Thickness – l	Curvature
164601	14	36	300
424321	15	21	1
620201	21	21	200
334165	12	15	1

Average thickness = 20
Thickness deviation = 6
Average curvature $\times 10^5$ = 120

Fig. XV-21. Computer analysis of "bow" sample.

curvature. It has been tested on several samples, and yields results that are in agreement with those obtained by visual estimation of these features, as can be seen in Fig. XV-21.

H. Levy, L. Stark

D. DIGITAL COMPUTER SIMULATION OF A NEUROLOGICAL SYSTEM

We have been simulating the control system for human movement coordination, using the BIOSIM program. This program provides for the simulation of a general class of dynamical systems from specifications of their block diagram representation and has been described previously.[1]

A block diagram for closed-loop operation of the postural muscular system and open-loop operation of the voluntary control system has been presented.[2] Its expanded and modified form is shown in Fig. XV-22.

The biological experiment is carried out by instructing the subject to hold his arm fairly tense and to maintain this position despite possible deflecting forces. A force of

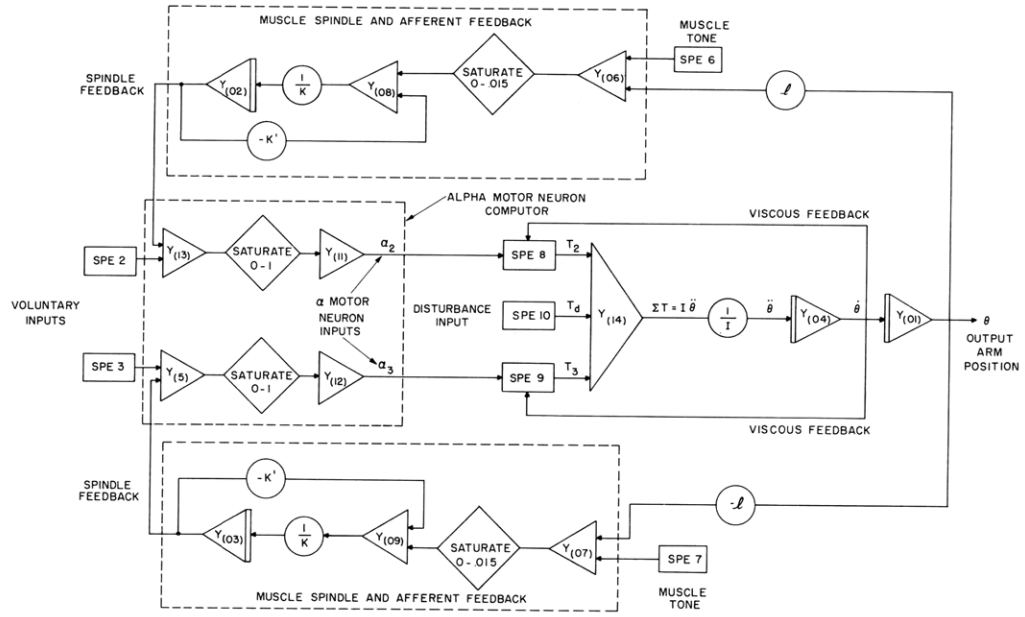

Fig. XV-22. BIOSIM block diagram of a simple motor coordination system. Constants: $I = 1/10 \frac{\text{kg-m}^2 \text{ sec}^2}{\text{rad}}$; $k = 0.0014 \frac{\text{m}}{\text{rad}}$; $k' = 0.014$ m; $\ell = 0.01$ meter; the initial condition on the integraters is zero.

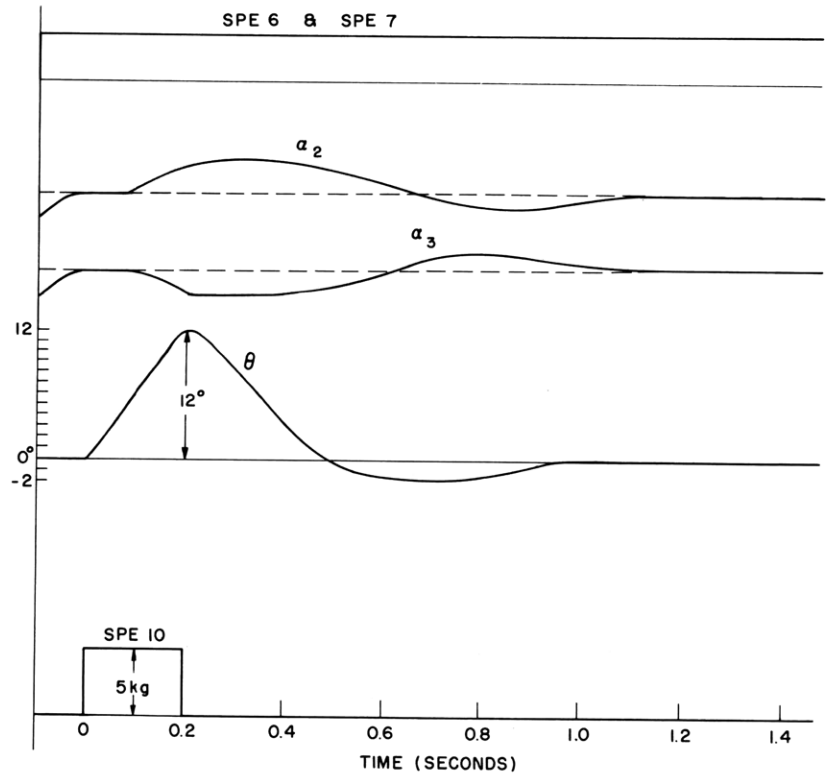

Fig. XV-23. BIOSIM outputs.

5 kg, lasting 0.2 sec, is applied. The subject's arm is deflected, and then returns to its desired position after a slight overshoot.

Table XV-2. Definitions of special functions.

Special Function (SPE)	Definition
SPE 6 and SPE 7	Muscle Tone = 0.001 u - 1(t)
SPE 8	$\begin{cases} -Y(11) + 100\ Y(11) * Y(13) & \text{if } Y(13) < 0 \\ -Y(11) + 600\ Y(11) * Y(13) & \text{if } Y(13) \geq 0 \end{cases}$
SPE 9	$\begin{cases} Y(12) - 600\ Y(12) * Y(05) & \text{if } Y(13) \geq 0 \\ Y(12) - 100\ Y(12) * Y(05) & \text{if } Y(13) < 0 \end{cases}$
SPE 10	Disturbing Force = $5[u-1(t)-u-1(t-0.2)]$
SPE 2 and SPE 3	Not used for this experiment

The BIOSIM analogy behaves as shown in Fig. XV-23. The tensing of the muscles is accomplished by inserting a bias signal using SPE 6 and SPE 7. (See Table XV-2.) The disturbing force is applied by means of SPE 10, and its time function is shown. As the hand is deflected from its zero position, the error signal of the stretched muscle increases and the error signal of the slackened muscle decreases. When the disturbing force ceases these signals, operating on their respective muscles, drive the hand back to its zero position with a slight overshoot. The initial biasing, hand position, disturbing force, and error signals are shown as time functions in Fig. XV-23, and indicate a qualitative and rough quantitative agreement with the experiment. In Fig. XV-23, α_2 represents input to muscle-restraining initial motion; α_3 represents input to muscle slackened by initial motion; θ represents deflection of the arm in degrees; and the dashed line indicates the bias level.

We are encouraged by these results and expect to pursue this model in the directions of: (a) better definition of the physical elements of the control system, (b) more accurate descriptions of system topology; and (c) further comparison with experiment.

J. Atwood, J. Elkind, J. Houk, M. King, L. Stark, P. A. Willis

References

1. V. W. Kipiniak, Simulation of biological control systems, Quarterly Progress Report No. 62, Research Laboratory of Electronics, M.I.T., July 15, 1961, pp. 284-286.

2. L. Stark, Neurological organization of the control system for movement, Quarterly Progress Report No. 61, Research Laboratory of Electronics, M.I.T., April 15, 1961, pp. 234-238.

E. INSTRUMENTATION FOR PROCESSING NEURAL SIGNALS*

Biological sensory receptors, acting as selective filters to the wide variety of energies available in the environment, transduce impingent energy into nerve pulse trains ("the neural code"). The pulse height or amplitude of the axone of a given sensory neuron (the "output") tends to be constant – obeying the "all-or-none" law. When the neuron population under study is small, differential pulse-height discriminators may be employed to single out and count those pulse-height groups carrying the transduced input signal.[1,2]

The ever-increasing use of electronic computers in neurophysiology calls for techniques that can flexibly digitize neural data. In the course of studying photoreception in the crayfish, we have developed a simple assembly of standard, low cost, readily available, and reliable components, which provide both pulse-height discrimination and digitization of raw nerve pulses. Naturally, the criterion of usage is sufficient pulse-height separability of units in the population, as well as separability in time – that is, the incidence of superimposition of one pulse on another should be negligible.

Table XV-3. Differential pulse-height counting.

Channel	Light Intensity (lux)	0	600	13,250	50,600
	Voltage Differential				
A	<50	1023	813	800	777
B	50-90	114	172	610	628
C	90-130	54	228	610	756
D	130-170	19	36	73	66
E	>170	12	9	25	35

The ventral abdominal photoreceptor in the crayfish has a population of less than 10 photosensitive neurons.[3] The axonic pulse-height amplitudes tend to be constant for each neuron, and cluster about an amplitude band that is separable from other (non-light responding) units as can be seen in Table XV-3. Further, the distribution in time is such that counting is possible. The low-amplitude pulses correlate inversely with the midrange (light) pulses.[4] When low and midrange pulses are counted together the sum shows less variation per change of input signal than counting the midrange group only.

*This research was supported by the U.S. Air Force under Contract AF-33(616)-7588, Project: 61(8-7232); Task 71784.

Reference to Fig. XV-26 illustrates the point. Here, the top trace formed by averaging pulse rates of all fibers shows less apparent gain than traces in which the low-voltage fibers are excluded by means of shifting the input bias level.

Averages of four experiments are presented. The numbers represent pulses counted over 15-sec intervals of illumination. Counting started at the moment of light "on" and continued for 15 seconds. For low illumination, the photoreceptor system has a 1-sec delay plus several seconds rise time to maximum. The latency period and rise time shorten with intensity.[4]

The decrease in low-voltage nerve pulses could be due to pre-empting of registers by the higher voltage pulses. However, we would not expect it at such low pulse rates. The pulse averages gave counts around 4000-8000 cpm, which agree with pulse counts made by our finer mesh system. Since the standard pulsewidth in our trigger system could be made arbitrarily small (up to 1 μsec) pulse superimposition coincidence (corresponding to pre-empting of registers in the Pulse-Height Discriminator) was negligible. Further, when the low-voltage pulses are summed with the midrange pulses the apparent gain is reduced and an inverse correlation between low voltage and midrange pulses is indicated.

Figure XV-24 illustrates the data flow of our instrumentation in block diagram form. Note that the computational components are separated from the pulse-selection, pulse-shaping components, so as to provide maximum flexibility of analysis. The assignment of the standard pulse to the nerve pulse is made in terms of the relation of the incoming

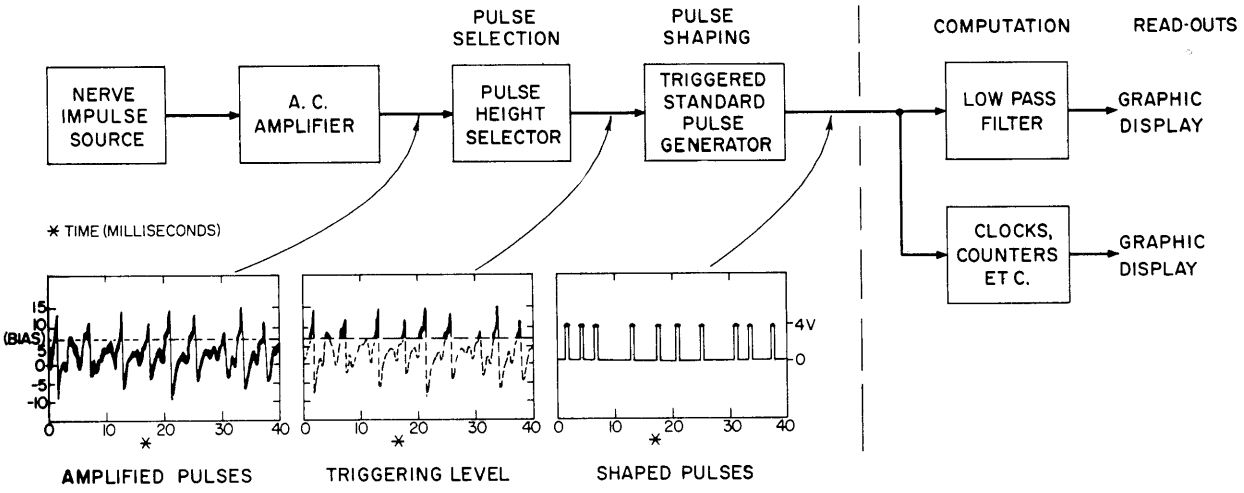

Fig. XV-24. Block diagram of instrumentation. Pulse-selection and pulse-shaping circuits are separate from computation circuits. In practice, lowpass filters are used to form an analog voltage corresponding to the instantaneous average frequency. A digital computer is used for interval analysis.

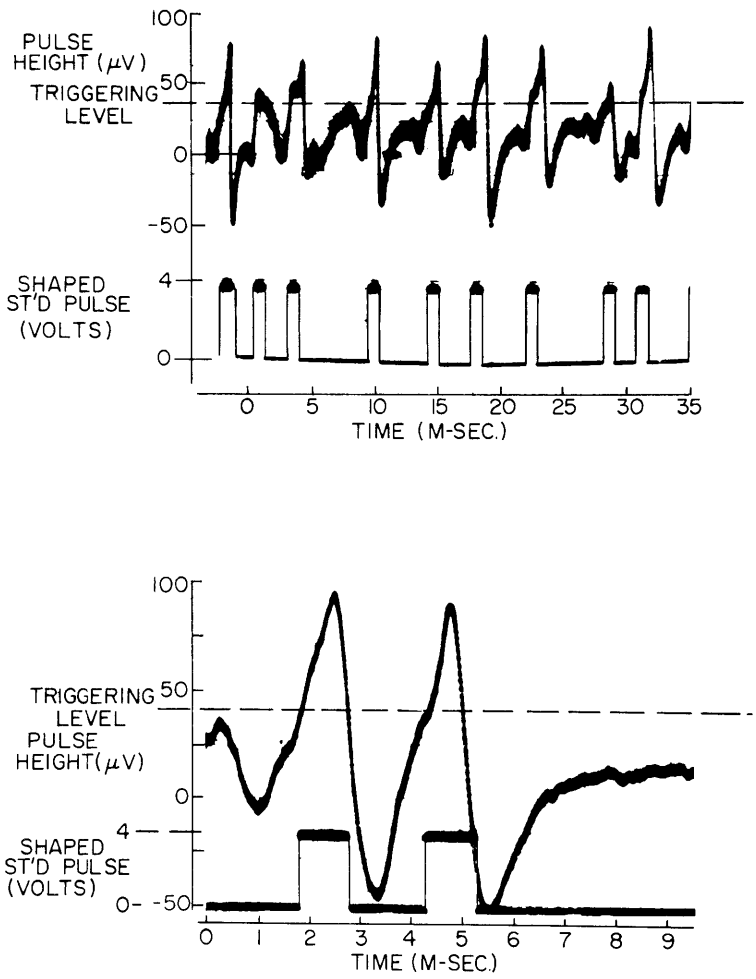

Fig. XV-25. Pulse selection and pulse shaping. (a) The relationship of nerve pulse and shaped pulse. Note that the standard shaped pulse initiates on the negative going slope (via the slope selector) of the nerve pulse. The dc level of triggering is set by a potentiometer in the cathode bias circuit. Conventional Schmitt triggers are employed (for example, Argonaut Associates triple-function generator). (b) The same sequence at higher gain and faster sweep.

pulse height to a preselected bias level. All pulses above a given bias level trigger a standard pulse (here, a 1-msec square wave of 4 volts). Figure XV-25 illustrates the assignment of shaped pulse to raw nerve pulse. One can also select the slope (positive or negative) on which a crossing of the bias level will fire the trigger. Thus, either the up- or the down-going part of a nerve pulse may be utilized as the trigger.

By passing the output of the pulse shapers through appropriate filters and clocks, pulse interval analysis, pulse height selection, autocorrelation, and crosscorrelation, and so forth, may be carried out with ease. We have utilized a lowpass filter whose time constant is long with respect to the pulse repetition rate, but short with respect to the

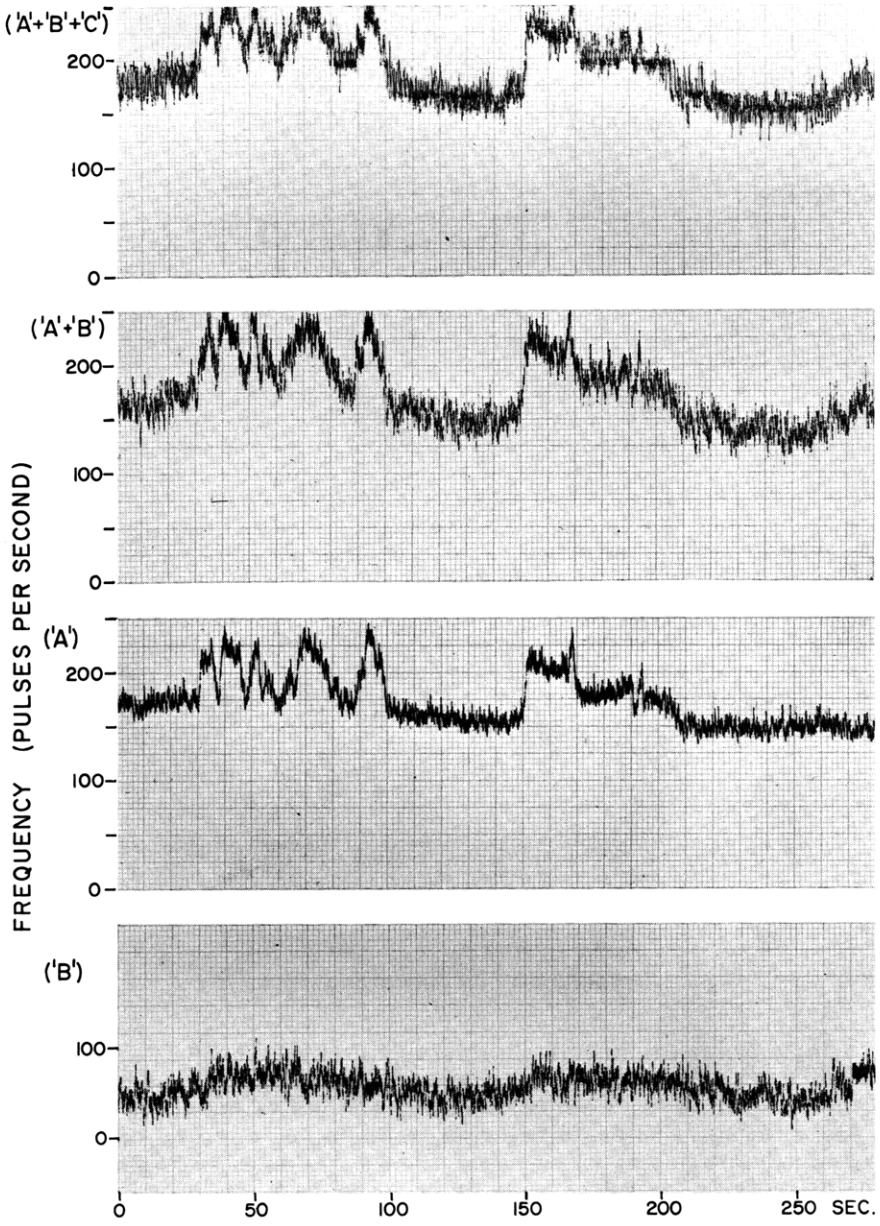

Fig. XV-26. Effect of screening out irrelevant pulses. The light stimulus is a sinusoidal fluctuation at 0.006 cps. The standard pulses have been passed through identical lowpass filters whose time constant (here, 0.20 sec) is long with respect to the average frequency of the pulses but short with respect to the response frequency of the photoreceptor.

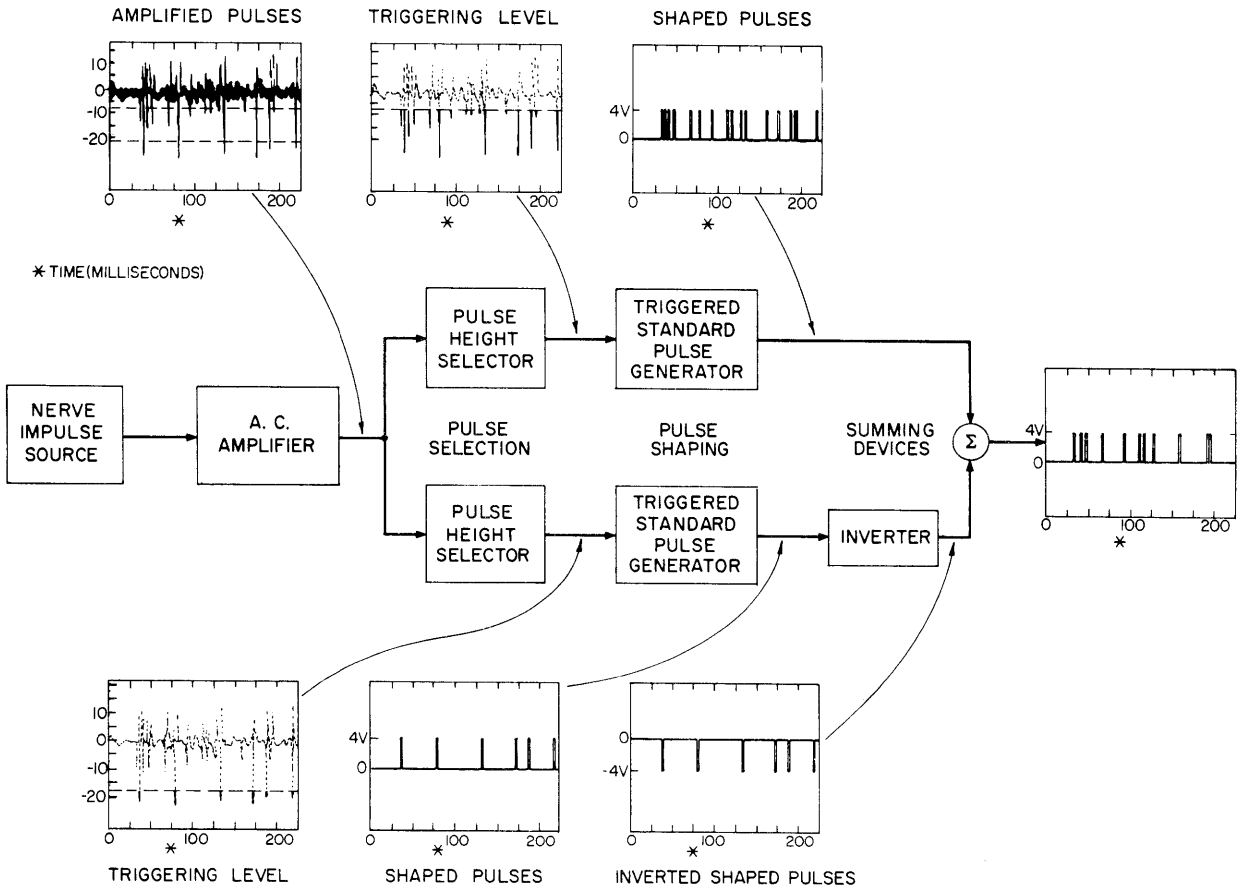

Fig. XV-27. Block diagram of the pulse-height "windows." On account of the difficulty of obtaining the necessary simultaneous oscillographic pictures, nerve pulses and corresponding shaped pulses are drawn in from actual recordings. The subtraction process is performed by summing the two inputs ("A") and ("B"), and ("-A") through a lowpass filter. Thus exact obliteration of one pulse by its negative counterpart is not necessary, since only the running average is recorded. Exact coincidence, of course, is impossible to achieve with this system, although close approximations can be made by introducing a delay into the lower triggering level and keeping the pulse width around 1 msec.

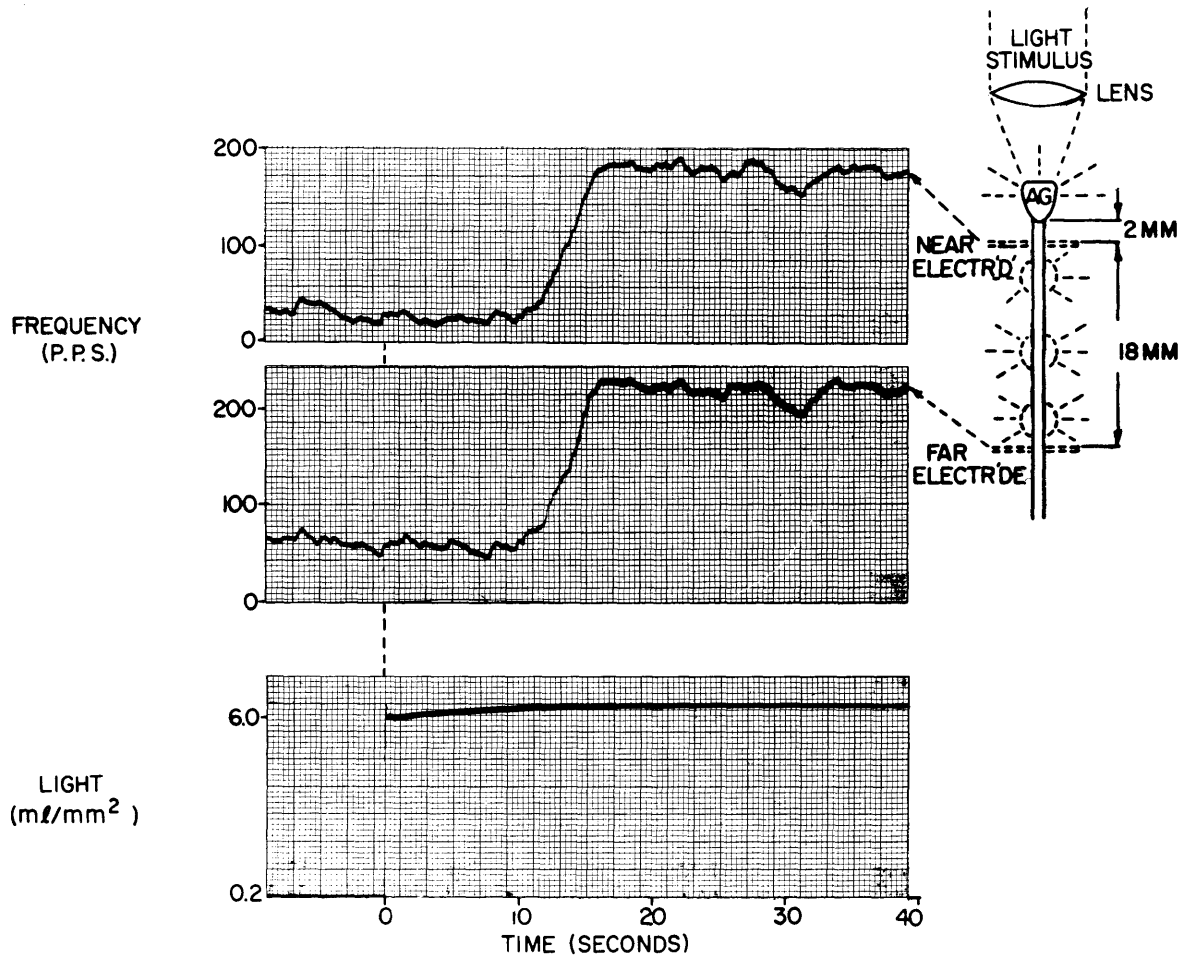

Fig. XV-28. Transient experiment. Electrodes were placed at two points on the ventral nerve cord of the crayfish. The two trigger systems were set at the same bias level. A sudden shift in light level produces the response, a rapid rise in pulse repetition rate. Note that the details of the response are recorded faithfully throughout the cord, despite change in geographic location and type of contact of the electrode. Synaptic relays, with attendant opportunity for convergence, divergence, and delay do not seem present. Cross-section variation in fiber location has negligible effect on the pulse-height characteristics of the responding fibers.

response frequency of the receptor as a means of generating an analog voltage corresponding to instantaneous average frequency.

We adjust the bias level by means of direct monitoring on an oscilloscope so that pulses are triggered only by those fibers that are under scrutiny. The effect of screening out irrelevant pulses (regarded here as "noise") may be seen in Fig. XV-26, trace 2 ('A'+'B') versus trace 4 ('B').

In many of our preparations we found higher amplitude pulses unrelated to the light signals. By stacking two trigger-shaper units in parallel, we were able to form a pulse height "window" that could be varied both in width and height. Figure XV-27 illustrates the block diagram of the "window." Subtraction was performed by passing the shaped pulses from the high-level trigger through a unity gain inverter, and adding the inverted pulses to the pulses from the lower level trigger. The effect of such screening can be seen in Fig. XV-26, trace 4 ('B'). The top trace ('A'+'B'+'C') illustrates the response characteristic of the total population. The apparent gain is reduced owing to the combined presence of the inversely correlating low and midrange pulses. The second trace ('A'+'B') shows the effect of screening out the low-voltage pulses. The apparent gain is increased now that the low-voltage pulses are excluded; the over-all pulse frequency drops. The third trace shows the responses of the units with pulse heights greater than 125 μv. As can be seen, no relevancy to the light fluctuation may be detected. The actual deflections are due to high-voltage pulses associated with a walk response in the crayfish. The fourth trace shows the effect of subtracting the third trace from the second trace. Note the reduction in noise, and the absolute reduction in frequency. The level of the trace was shifted up so as to center the record.

It should be added parenthetically that the relative displacement of the light-carrying fibers with regard to the recording electrode had little or no effect on the average frequency determination of the output. Figure XV-28 shows that the signal is preserved with remarkable constancy throughout the cord. Clearly no synapses exist. Furthermore, changes in impedance between pulse emf source and the electrode, caused by shifts in cross-section location of the emf source, are far smaller than the total impedance interposed between the recording electrode and the indifferent electrode.[5] Thus pulse-height selection is negligibly influenced by the location of the electrode under ordinary macroelectrode recording conditions.

Conclusion

When nerve populations are small, such that one can neglect the incidence of exact superimposition of one pulse on another in time or in amplitude, differential pulse-height analysis is possible. It offers a low-cost, easy, and reliable method of increasing signal extraction from irrelevant accompanying signals. In effect, one employs electronic "nerve dissection." Another advantage is that of flexible digitization of data.

Acknowledgment

We wish to acknowledge the valuable advice and help of Dr. Charles Walcott, of the Department of Biology, Harvard University, in stimulating the design of our equipment.

H. T. Hermann, L. Stark, P. A. Willis

References

1. R. Littauer and C. Walcott, Five channel differential pulse height analyzer, Rev. Sci. Instr. 30, 1102 (1959).

2. C. Walcott and W. C. van der Kloop, The physiology of the spider vibration receptor, J. Exp. Zool. 141, 191-244 (1959).

3. D. Kennedy, Responses from the Crayfish Caudal Photoreceptor, Am. J. Opthalmol. 11, 19-26 (1958).

4. L. Stark and H. T. Hermann, Light transfer function of a biological photoreceptor, Quarterly Progress Report No. 62, Research Laboratory of Electronics, M. I. T., July 15, 1961, pp. 251-255.

5. H. T. Hermann and L. Y. Young, Field Recording Characteristics of Macro-electrodes in Volume Conductors (In preparation).